Design of a Simulated Moving Bed in the Presence of Mass-Transfer Resistances

Diana C. S. Azevedo and Alírio E. Rodrigues
Laboratory of Separation and Reaction Engineering (LSRE), Faculty of Engineering, University of Porto, 4099 Porto Codex, Portugal

Two different strategies presented determine the sets of operating conditions that yield desired product purities for an SMB separator. The search was performed numerically by solving the analogous true-moving-bed model equations. A linear equilibrium binary mixture and mass-transfer effects were taken into account by using a bilinear driving force approximation to describe intraparticle diffusion. The strategies are equivalent and produce the same results. Comparison with the linear equilibrium model strategy indicates that there are new limiting values for the flow-rate constraints in the presence of mass-transfer effects. The constraints on sections I, II and III were more restrictive than those derived from equilibrium models, whereas the constraint on section IV was less affected. Qualitative observations drawn from a model of intermediate complexity were also presented to confirm our results.

Introduction

The simulated moving-bed (SMB) technology was first patented by Universal Oil Products (UOP) in 1961 (Broughton, 1961) and, since then, it has found increasingly new applications in the areas of biotechnology, pharmaceuticals, and fine chemistry (Humphrey, 1995). SMB technology was first conceived for bulk large-scale separations, in which the solid movement was accomplished by means of a rotary valve that periodically shifted the feed, eluent, raffinate, and extract lines along the bed. This was known as SORBEX technology (Rosset et al., 1981; Johnson, 1989; Johnson and Kabza, 1993), which included the Parex process for *p*-xylene separation from C8 aromatics, the OLEX process to separate olefins from paraffins, the SAREX process to separate fructose from glucose for HFCS production, among others.

As new preparative chromatographic applications were discovered, the physical configuration of an SMB unit changed to a set of fixed beds (see Figure 1) connected in series segmented by valves and inlet/outlet lines (Keller, 1995). Countercurrent motion of the solid was simulated by convenient actuation of these valves so that, from time to time, the inlet and outlet streams were switched in the direction of fluid-phase flow.

Due to its complex physical configuration, the modeling, simulation, and design of an SMB unit prior to plant operation is a necessary but not straightforward task. Many authors have proposed theoretical models to describe the performance and internal profiles of SMB units (Ruthven and Ching, 1989; Storti et al., 1989; Ernst and Hsu, 1989; Zhong and Guiochon, 1996; Strube et al., 1997; Pais et al., 1998). In general, the modeling approaches may be grouped into two categories: those that represent the actual simulated moving-bed configuration (with periodically changing bed boundary conditions) and those that represent the equivalent true moving bed (TMB) (with the coupling of four countercurrent sections). The main difference between these two approaches is that the steady state can be obtained only in an asymptotic sense in SMB, while it is a definite state in TMB (Zhong and Guiochon, 1998). The raffinate and extract steady-state concentrations actually vary periodically in a cycle, but the average concentrations in a period are practically the same as those obtained for the TMB. Therefore, even though small differences will appear between these two strategies, the prediction of the performance of an SMB operation can be done using the TMB approach (Pais et al., 1998).

Correspondence concerning this article should be addressed to A. E. Rodrigues.
D. C. S. Azevedo is on leave from GPSA, Department of Chemical Engineering, Federal University of Ceará (Brazil).

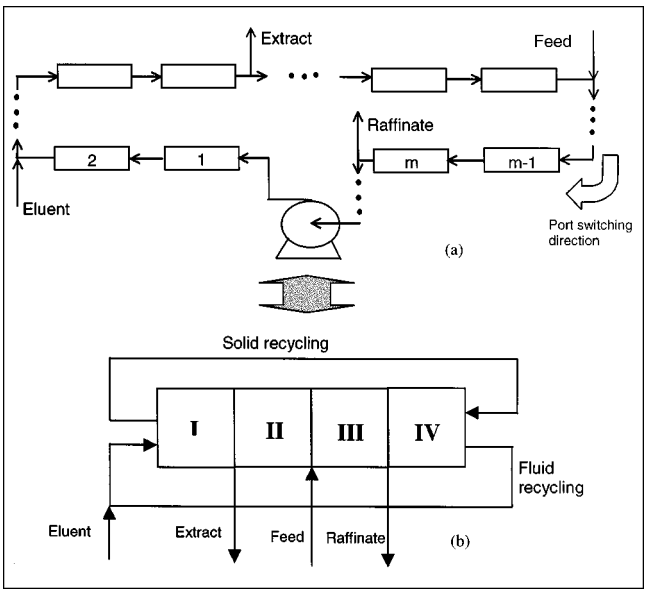

Figure 1. (a) Simulated moving bed (SMB); (b) true moving bed (TMB).

They are equivalent according to the relations in Table 1.

It has also been shown that there are certain flow-rate restrictions that must be fulfilled for the desired separation to occur. These restrictions must be such that the more strongly retained component(s) present in the mixture move in the direction of the extract port. Accordingly, the less retained component(s) should be collected in the raffinate port. These flow-rate restrictions can be easily found if an ideal situation is considered (axial mixing and mass-transfer resistances neglected). They have been established in the literature for linear and Langmuir-type isotherms (Storti et al., 1993; Fish et al., 1993; Mazzotti et al., 1996, 1997; Zhong et al., 1997). Although equilibrium models are a powerful design tool, the conditions for separation may not fully apply in the design of real SMB units since dispersion and mass-transfer effects are very frequently present. Furthermore, the assumption of instantaneous surface equilibrium may not be realistic in some cases, especially when dealing with proteins and macromolecules (Mian et al., 1998). So far, these effects have been taken into account by using a safety margin factor (β) in the equilibrium models, whose value is attributed randomly and may lead to over- or underestimating errors. The first attempt to introduce mass-transfer effects into SMB design was proposed by Pais et al. (1997), who described intraparticle mass transfer with a simple LDF approximation. It was shown that the set of values of fluid/solid flow-rate ratios in sections II and III ($\gamma_2 \times \gamma_3$) that yield separation are considerably reduced when mass-transfer effects are present.

The objective of this work is to present two strategies for the optimization of SMB operating conditions, which take mass-transfer effects into account. The intraparticle mass transfer is described by a bi-LDF approximation (Azevedo and Rodrigues, 1998). A linear equilibrium binary mixture is considered. The influence of the mass-transfer effects on the flow-rate restrictions is examined in each SMB zone and compared to the restrictions obtained from equilibrium models. For the sake of validation of this optimization strategy, an analytical solution for a model of intermediate complexity (linear equilibrium, single mass-transfer time constant) is examined and compared with our numerically simulated results.

Table 1. Equivalence Relations between SMB and TMB Title

	SMB	TMB
Solid phase:		
Velocity	0	$U_S = L/t^*$
Flow rate:	0	$Q_S = U_S(1-\epsilon)A$
Liquid phase:		
Velocity:	v_j^*	$v_j = v_j^* - U_S$
Flow rate:	Q_j^*	$Q_j = Q_j^* - \epsilon V/t^*$

Source: Leão et al. (1987).

Mathematical Model

The operating conditions of an SMB separator were optimized by solving the equivalent TMB model. Figure 1 shows the representation of both SMB and TMB, and Table 1 shows the equivalence relations between them.

The mathematical model proposed to represent the steady state in a section j of a true countercurrent unit is presented in Eqs. 1 to 15. Axially dispersed flow is assumed for the fluid phase and plug flow for the solid phase. Diffusion through the external film is also considered, and intraparticle mass transfer is represented by means of a bilinear driving force described elsewhere (Azevedo and Rodrigues, 1998).

- Mass balance in outer fluid phase:

$$\frac{\gamma_j}{Pe_j}\frac{\partial^2 C_j}{\partial x^2} - \gamma_j\frac{\partial C_j}{\partial x} - \frac{(1-\epsilon)}{\epsilon}\left[\frac{Bi_{mj}}{5+Bi_{mj}}\alpha_{pj}\left(C_j - \overline{C}_{pj}\right)\right] = 0. \tag{1}$$

- Mass balance in intraparticle fluid phase (pores):

$$\frac{\partial \overline{C}_{pj}}{\partial x} + \frac{Bi_{mj}}{5+Bi_{mj}}\frac{\alpha_{pj}}{\epsilon_p}\left(C_j - \overline{C}_{pj}\right) - \frac{\alpha_{\mu j}}{\epsilon_p}\rho_p\left[\frac{K}{\rho_p}\overline{C}_{pj} - \langle \overline{q}\rangle_j\right] = 0. \tag{2}$$

- Mass balance in intraparticle "solid" phase (microparticles):

$$\frac{\partial \langle \overline{q}\rangle_j}{\partial x} + \alpha_{\mu j}\left[\frac{K}{\rho_p}\overline{C}_{pj} - \langle \overline{q}\rangle_j\right] = 0. \tag{3}$$

- Boundary conditions for section j:

  at $x = 0$

$$C_j^{\text{in}} = C_j(0) - \frac{1}{Pe_j}\frac{\partial C_j}{\partial x}; \tag{4}$$

at $x = 1$

$$\frac{\partial C_j}{\partial x}(1) = 0 \tag{5}$$

$$\overline{C}_{pj}(1) = \overline{C}_{p(j+1)}(0) \tag{6}$$

$$\langle \overline{q} \rangle_j(1) = \langle \overline{q} \rangle_{j+1}(0). \tag{7}$$

The dimensionless space variable is $x = z/L_j$, where L_j is the length of section j. The dimensionless numbers present in the model equations are:

$$\gamma_j = \frac{U_{Fj}}{U_S} \quad \text{Fluid/solid interstitial velocity ratio} \tag{8}$$

$$\alpha_{pj} = \frac{k_p L_j}{U_S} \quad \text{Number of macropore mass-transfer units} \tag{9}$$

$$\alpha_{\mu j} = \frac{k_\mu L_j}{U_S} \quad \text{Number of microparticle mass-transfer units} \tag{10}$$

$$Bi_{mj} = \frac{k_{fj} R_p}{D_{pe}} \quad \text{Mass Biot number (film diffusion/effective pore diffusion)}. \tag{11}$$

C^{in} present in the boundary condition at the section inlet can be found from the node balances.

Eluent node:

$$C_{\text{I}}^{\text{in}} = \frac{Q_{\text{IV}}}{Q_{\text{IV}} + Q_E} C_{\text{IV}}(1). \tag{12}$$

Extract node:

$$C_{\text{II}}^{\text{in}} = C_{\text{I}}(1). \tag{13}$$

Feed node:

$$C_{\text{III}}^{\text{in}} = \frac{Q_{\text{II}}}{Q_{\text{III}}} C_{\text{II}}(1) + \frac{Q_F}{Q_{\text{III}}} C_F. \tag{14}$$

Raffinate node:

$$C_{\text{IV}}^{\text{in}} = C_{\text{III}}(1). \tag{15}$$

Optimization of SMB Operating Conditions

Optimizing the operation of an SMB consists in predicting the operating conditions (flow rates, rotation period) that yield, given a physical configuration of columns, a better separation at minimum cost. In other words, it is desirable to maximize the purity and recovery of products, making effective use of the adsorbent while minimizing the solvent consumption. Therefore, the optimization procedure may intend to minimize and/or maximize one or more performance criteria. As far as this work is concerned, the strategies of optimization used have attempted to maximize product purity, that is, find the compromise between section flow-rate ratios that would result in purities above 99% for both extract and raffinate. Depending on the purpose of a given SMB separation process, other criteria (recovery, productivity) may be more relevant than the one used here.

For separation of a binary mixture to occur, each of the four sections of the SMB must perform a certain role. If a binary mixture of A (more strongly adsorbed component) and B (more weakly adsorbed component) is fed in an SMB, A will only move toward the extract port and B to the raffinate port if certain restrictions are met. Next, these conditions will be stated, bearing in mind the analogous representation of a true moving bed (see Figure 1).

Section I is the adsorbent regeneration zone. The more retained component, A, must be displaced by the eluent (solvent) to the fluid phase. Therefore, the net flow of A must be that of the fluid phase. In section II, between extract and feed nodes, desorption of the weakly adsorbed component, B, happens. The net flux of B must be that of the fluid phase. Section III is where A is adsorbed. It must, then, move with the solid phase. In section IV, the solvent is regenerated and the less retained component, B, is adsorbed. The net flux of B must be that of the solid phase. These movement constraints may be expressed as the following:

$$\frac{Q_{\text{I}} C_{\text{A,I}}}{Q_S \rho_p q_{\text{A,I}}} > 1 \tag{16}$$

$$\frac{Q_{\text{II}} C_{\text{B,II}}}{Q_S \rho_p q_{\text{B,II}}} > 1; \qquad \frac{Q_{\text{II}} C_{\text{A,II}}}{Q_S \rho_p q_{\text{A,II}}} < 1 \tag{17}$$

$$\frac{Q_{\text{III}} C_{\text{B,III}}}{Q_S \rho_p q_{\text{B,III}}} > 1; \qquad \frac{Q_{\text{III}} C_{\text{A,III}}}{Q_S \rho_p q_{\text{A,III}}} < 1 \tag{18}$$

$$\frac{Q_{\text{IV}} C_{\text{B,IV}}}{Q_S \rho_p q_{\text{B,IV}}} < 1, \tag{19}$$

where $\rho_p q$ refers to the amount present inside the particle, which includes both the amount present in the macropores and the amount present in the microparticles. For a linear isotherm $\rho_p q = \rho_p \langle \overline{q} \rangle + \epsilon_p \overline{C}_p$. If resistances to mass transfer are ignored, $\rho_p \langle \overline{q} \rangle = K \overline{C}_p$ and $\overline{C}_p \cong C$, so that $\rho_p q/C = K + \epsilon_p = K'$. Note that $\gamma_j = U_{Fj}/U_s$ for a given section j, so that the constraints written previously can be reduced to

$$\gamma_1 > \nu K'_{\text{A}} \tag{20}$$

$$\nu K'_{\text{B}} < \gamma_2 < \nu K'_{\text{A}} \tag{21}$$

$$\nu K'_{\text{B}} < \gamma_3 < \nu K'_{\text{A}} \tag{22}$$

$$\gamma_4 < \nu K'_{\text{B}}, \tag{23}$$

where $\nu = (1 - \epsilon)/\epsilon$ and $\gamma_3 > \gamma_2$.

These constraints define separation in an SMB for a linear equilibrium binary system in the absence of dispersion and mass-transfer effects. They are in accordance with the equi-

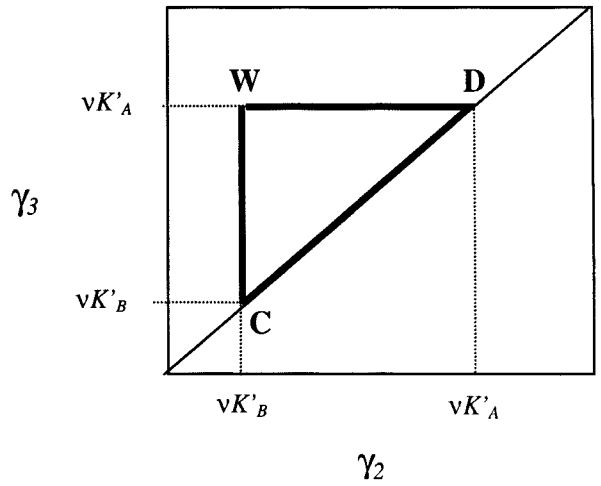

Figure 2. Region of separation (pure extract and raffinate) in a $\gamma_2 \times \gamma_3$ plane.

librium model results first proposed by Storti et al. (1993). In a $\gamma_2 \times \gamma_3$ *plane*, this region corresponds to the triangle CWD shown in Figure 2. Inside this triangle, provided the constraints on γ_1 and γ_4 are not violated, any (γ_2, γ_3) pair yields separation.

The equilibrium model predicts that, for any values of γ_1 and γ_4 (in accordance with Eqs. 20 and 23, respectively), the region of separation in a $\gamma_2 \times \gamma_3$ plane will be constant and defined only by the solid/fluid volume ratio, ν, and the equilibrium constants. However, when mass-transfer resistances are significant, the term $\rho_p q = \rho_q \langle \bar{q} \rangle + \epsilon_p \bar{C}_p$ cannot be simplified as shown previously, and the constraints are not as explicit as in Eqs. 20 to 23. The separation region is expected to become narrower and the new constraints should be dependent on mass-transfer rate constants.

The dependency of flow-rate constraints on mass-transfer effects may be more clearly verified from a qualitative examination of a TMB simplified model. Let us consider the two sections where separation actually occurs, that is, sections II and III, as shown in Figure 3. For the sake of simplicity, axial dispersion will be neglected and only one mass-transfer resistance will be taken into consideration.

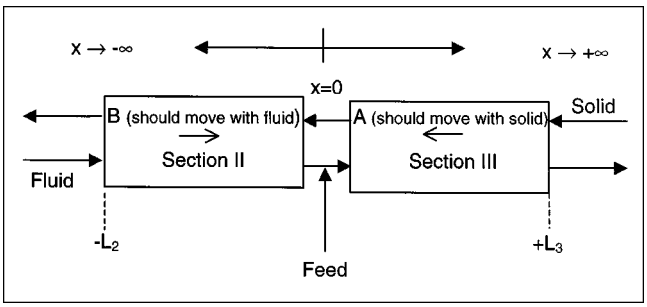

Figure 3. Net flow of A and B in sections II and III, where separation actually occurs.

Using the same boundary conditions as proposed by Ma and Wang (1997), the analytical solutions for the bulk fluid-phase concentration lead to Eqs. 24 and 25. For a detailed derivation of the analytical solution, refer to the Appendix. The equations refer to species B (weakly adsorbed component) in section II and species A (strongly adsorbed component) in section III, which impose the relevant restrictions in these sections for separation to occur:

$$\beta_{B,II} = \frac{C_{B,II}(x=0)}{C_{B,II}(x=-1)} = \exp\left(\frac{\alpha(\gamma_2 - \nu K_B)}{\gamma_2}\right) \quad (24)$$

$$\beta_{A,III} = \frac{C_{A,III}(x=0)}{C_{A,III}(x=1)} = \exp\left(\frac{\alpha(\nu K_A - \gamma_3)}{\gamma_3}\right). \quad (25)$$

Rearranging the preceding equations in terms of γ_2 and γ_3:

$$\gamma_2|^{\min} = \frac{\alpha}{-\ln \beta_{B,II} + \alpha} \nu K_B = \frac{\alpha}{-\ln \beta_{B,II} + \alpha} \gamma_2|_{eq}^{\min} \quad (26)$$

$$\gamma_3|^{\max} = \frac{\alpha}{\ln \beta_{A,III} + \alpha} \nu K_A = \frac{\alpha}{\ln \beta_{A,III} + \alpha} \gamma_3|_{eq}^{\max}, \quad (27)$$

where $\gamma_2|_{eq}^{\min}$ and $\gamma_3|_{eq}^{\max}$ are the minimum and maximum bounds for γ_2 and γ_3 as given by the equilibrium model, respectively. Depending on the value of $\ln \beta$, the new constraints may be greater or less than the value from the ideal model. For section II, the fluid-phase concentration of B at $x = 0$ should always be greater than at $x = -1$, so that $\ln \beta_{B,II} > 0$. The same is true for species A in section III, so that the following are true:

$$\gamma_2|^{\min} > \gamma_2|_{eq}^{\min} \quad (28)$$

$$\gamma_3|^{\max} < \gamma_3|_{eq}^{\max}. \quad (29)$$

When the number of intraparticle mass-transfer units is too large ($\alpha \to \infty$), the flow-rate constraints become those derived from the equilibrium theory. In a $\gamma_2 \times \gamma_3$ plane, the new region of separation, which is dependent on mass-transfer effects, is narrower than that defined by the ideal model, as shown in Figure 4.

From these results it is clear that, if a certain performance is required from an SMB (for instance, in terms of product purity), the flow-rate constraints in a given section do not only depend on equilibrium of adsorption data, they also depend on the solid velocity (rotation period), section length, and the mass-transfer time constants. This prevents us from obtaining explicit flow-rate ratio limits from which to design optimum or robust operation, as is easily done with ideal linear equilibrium systems. Therefore, when mass-transfer effects are present, it is possible to define the regions of separation in terms of flow-rate ratio constraints through simulation. In the following sections, results from optimization procedures, based on two strategies, are presented in order to verify some of these qualitative observations mentioned earlier.

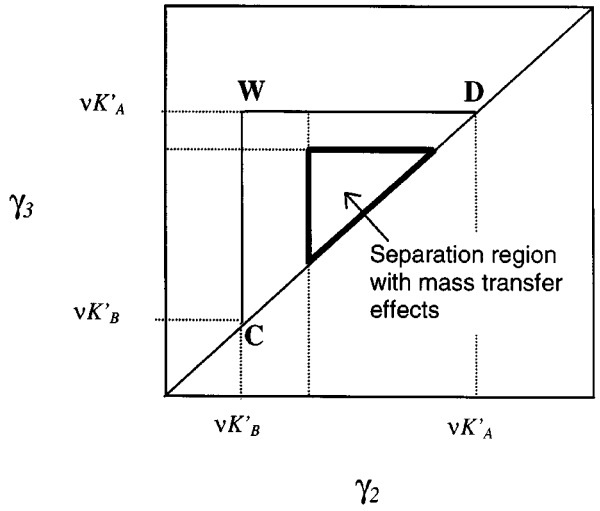

Figure 4. Region of separation with mass-transfer effects considered.

Results and Discussion

In order to analyze the influence of mass-transfer effects on the region of separation, the TMB steady-state model, as described in Eqs. 1 through 15, was successively solved for several values of (γ_2, γ_3) within the equilibrium separation region. The strategy used to find this region of separation consisted in fixing values for the rotation period, recycle flow rate, and sum of inlet/outlet streams ($QBAL = Q_F + Q_E = Q_X + Q_R$). The recycle flow rate was taken as the flow rate in zone IV, so that, for each optimization procedure, γ_4 was established. Then, following a given order determined by successive increments, values of (γ_2, γ_3) were simulated within the region of separation as given by the equilibrium model. The values of γ_1 varied for each simulation according to Eq. 30, and care was taken so that the constraint on γ_1, as given from Eq. 20, was not violated. Figure 5 summarizes the strategy used to find the region of separation, taking mass-transfer effects into consideration. The increment Δ in γ_2 and γ_3 was also attributed by the user of the optimization package and a typical value of 0.01 was used:

$$QBAL = \frac{\epsilon V_c}{t^*}(\gamma_1 - \gamma_4 + \gamma_3 - \gamma_2). \qquad (30)$$

For each optimization procedure as described previously, those values of (γ_2, γ_3) that resulted in purities above 99% for both extract and raffinate were selected to build a new region of separation. The values that did not fulfill this requirement were discarded. The resulting region of separation for fructose(A)/glucose(B) separation are shown in Figure 6 for different values of α_p and α_μ. The column configuration and equilibrium data are shown in Table 2.

Figure 6a compares the different regions of separation obtained for a fixed value of $\alpha_p = 23$. For both Figures 6a and 6b, γ_4 was set to 0.155 and γ_1 was calculated for each pair (γ_2, γ_3) according to Eq. 30. For $\alpha_\mu = 200$, the region of separation approaches that given from an equilibrium model

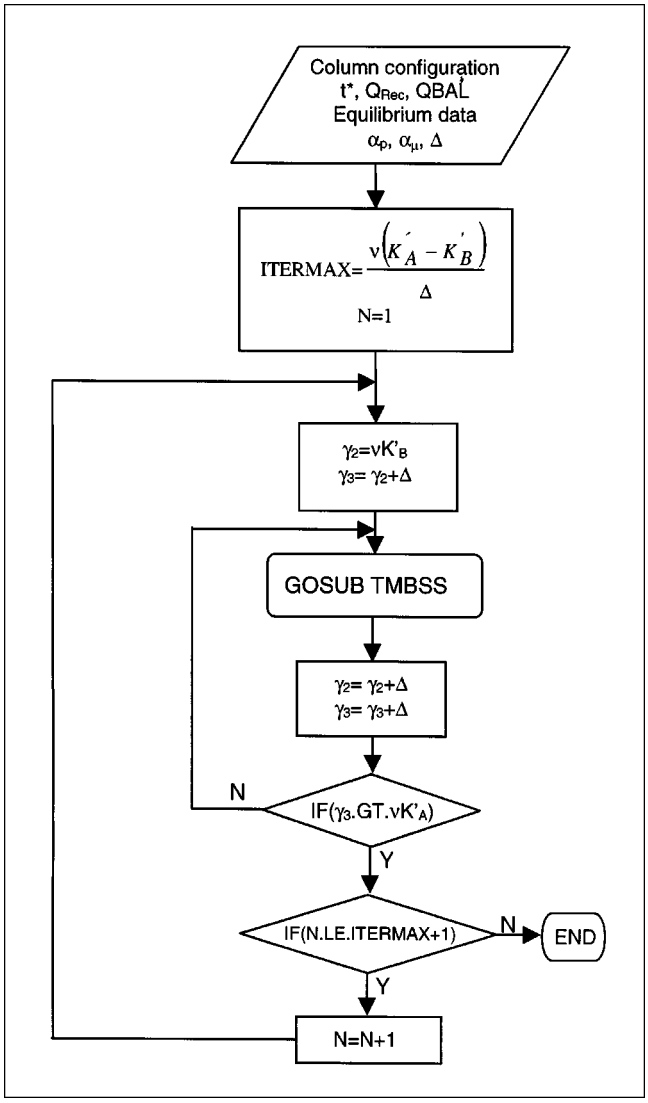

Figure 5. Simplified algorithm for the numerical determination of the region of separation.

(Figure 2). In this case, mass-transfer resistance in the microparticles is negligible, but there is still some resistance in the pores. Therefore, the region of separation is smaller than the triangle defined by the ideal linear model. As resistances to mass transfer are added, that is to say, as α_μ decreases, the region of separation becomes narrower and disappears for α_μ below 10. Figure 6b shows the regions of separation obtained for a constant value of $\alpha_\mu = 10$ and values of α_p ranging from 23 to 360. The values of α_p correspond to particle radius within the range of 50 to 200 μm, inside which molecular diffusivity is assumed with a tortuosity factor of 2. A similar behavior is observed in relation to Figure 6a. As α_p increases, global resistance to mass transfer decreases. As a result, the region of separation expands and tends to assume a fixed size, which is still quite different from the ideal linear equilibrium region. For both Figures 6a and 6b, one of the two mass-transfer resistances (α_p or α_μ) is negligible in relation to the other in the extreme cases, that is, $\alpha_p = 23/\alpha_\mu =$

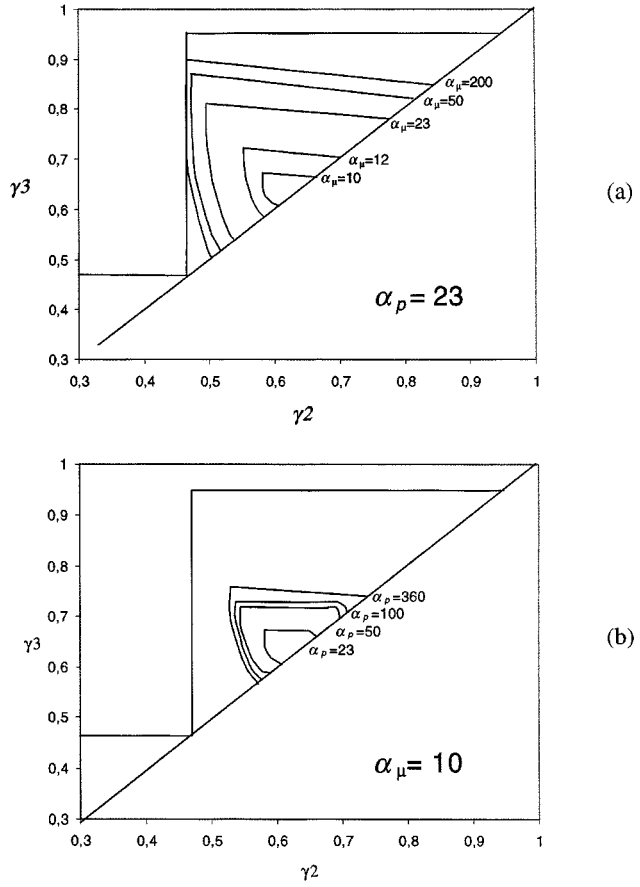

Figure 6. Regions of separation for: (a) a fixed α_p; (b) a fixed α_μ.

Column configuration and other relevant information on this optimization procedure are shown in Table 2.

200 for Figure 6a and $\alpha_p = 360/\alpha_\mu = 10$ for Figure 6b. In such cases, the bi-LDF approximation can be reduced to a simple LDF expression (Azevedo and Rodrigues, 1998), and comparison with the qualitative observations presented previously is pertinent. As predicted from the analytical solution, the limits for the region of separation are narrower as compared to the region of separation given by the ideal equilibrium model. These new bounds are dependent on mass-transfer effects and, as new kinds of diffusion resistances are added, this ''shrinking'' effect becomes more pronounced. It should be pointed out that these separation regions can only be of use for optimization and design purposes for a given value of α_p and α_μ. These dimensionless numbers are a function of solid interstitial velocity and zone length. Therefore, a different ratio (L_j/U_s) from the one used in Figure 6 may not result in complete separation, even if flow-rate ratios from inside the separation region are used. If mass-transfer effects are involved, even a small change in the rotation period, while maintaining the same zone length, may cause the components not to flow toward the raffinate and extract ports, as previously described.

Table 2. Model Parameters and Operating Conditions Used in Simulations

Model Parameters	Operating Conditions	Columns
$Pe = 2{,}000$	$T = 20$°C	$D_c = 2.6$ cm
$Bi_m = 500$	Feed concentration, $C_F = 30$ g/L each	$L_c = 11.5$ cm
$2.3 \le k_p \le 10$ min^{-1}	$t^* = 3.3$ min	Configuration: 3-3-3-3
$0.4 \le k_\mu \le 1.2$ min^{-1}	$Q_{\text{Rec}} = 8.55$ mL/min	Zone length = 34.5 cm
$K_{FR} = 0.435$	$\gamma_4 = 0.155$	
$K_{GL} = 0.114$	$QBAL = Q_F + Q_E = 11$ mL/min	

The influence of mass-transfer effects on the restrictions of sections I and IV was also examined. This was also done through numerical simulation in order to find a three-dimensional separation *volume*, instead of a two-dimensional separation *area*. Two strategies were used to find these *separation volumes*, namely, strategy 1 and strategy 2. The objective of both strategies was to find the sets of points ($\gamma_1/QBAL$, γ_2, γ_3) in a three-dimensional space that resulted in purities above 99% for both raffinate and extract streams. Both procedures were applied for a given fixed value of γ_4 lower than $\nu K'_B$, according to the equilibrium constraint given in Eq. 23.

For strategy 1, values of γ_1 were attributed to a minimum of $\nu K'_A$ (constraint in Eq. 20) and gradually incremented according to the optimization package user. For each value of γ_1, the steady-state performance of the SMB was simulated for different values of γ_2 and γ_3 within the range of $[\nu K'_B, \nu K'_A]$. Figure 7 shows the algorithm used for this new strategy.

This optimization procedure was performed for three values of γ_4 (0.155, 0.290, and 0.392), all of which obeyed the equilibrium constraint as given in Eq. 23. The obtained regions of separation in a three-dimensional system of coordinates are shown in Figures 8, 9, and 10 for $\gamma_4 = 0.155$, 0.290, and 0.392, respectively. The blue plane represents the $\gamma_2 = \gamma_3$ plane. The two-dimensional views $\gamma_1 \times \gamma_2$, $\gamma_1 \times \gamma_3$, and $\gamma_2 \times \gamma_3$ are also shown for each of the figures. The minimum value shown on the γ_1 axis for all graphs is $\nu K'_A$, that is, the equilibrium constraint value as given in Eq. 20. It is interesting to note that the regions of separation only occur at approximately $\gamma_1 = 1.20$, which is considerably greater than $\nu K'_A$ (= 0.95). Another indication is that the regions of separation only have a constant size at γ_1 greater than 1.60. There is a kind of ''transition region'' ($1.20 < \gamma_1 < 1.60$), in which the regions of separation have varying size, probably dependent on the mass-transfer effects. The figures also show that γ_4 does not affect significantly the size of the separation region, except in the ''transition region.''

For strategy 2, the same methodology as described in strategy 1 was applied, but $QBAL$ ($= Q_F + Q_E = Q_X + Q_R$) was incremented instead of γ_1. In fact, this strategy is an extension of that described in the flow sheet shown in Figure 5, for which a single value of $QBAL$ is tested. Because there is a compromise between $QBAL$, γ_1, γ_2, γ_3, and γ_4 (given by Eq. 30), both strategies 1 and 2 are expected to yield the same results. To compare the two strategies, the region of separation for $\gamma_4 = 0.290$, $\alpha_p = 200$, and $\alpha_\mu = 12$ was searched using the two procedures. The results are shown in Figure 11. It is difficult to compare them in such a representation, as the *y*-axis stands for γ_1 in one graph and $QBAL$ in the other graph. In order to verify clearly the equivalence between the

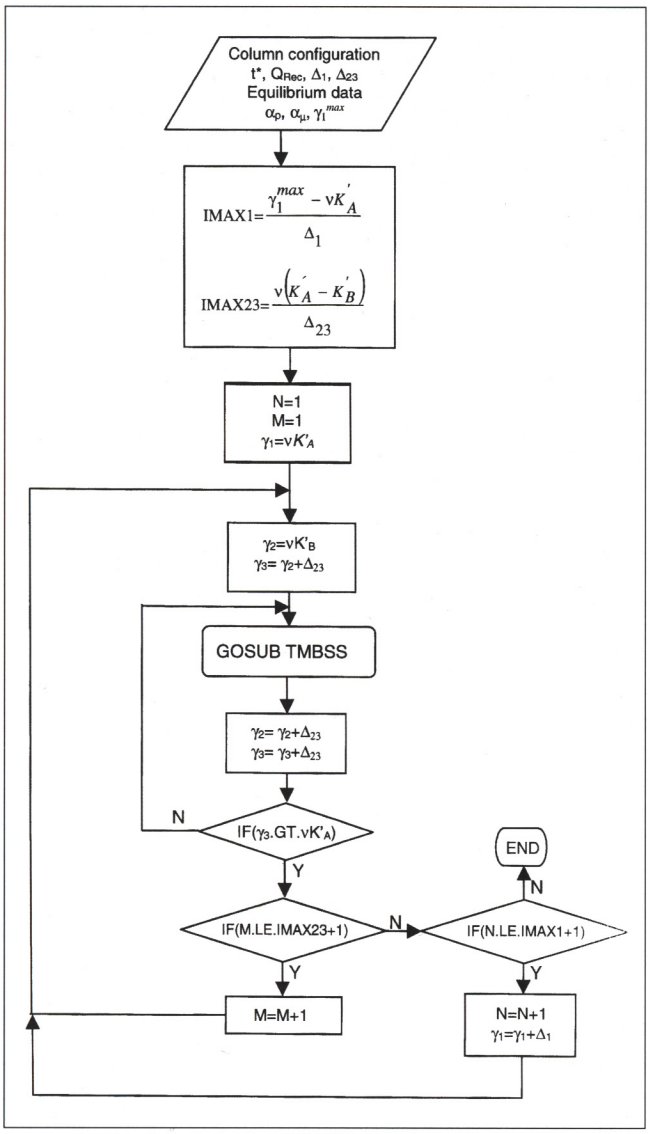

Figure 7. Simplified algorithm for the numerical determination of the region of separation in a three-dimensional space.

two strategies, some points from the graph 11a were chosen so that the calculated values of *QBAL* (from Eq. 30) were equal to 11 mL/min. These selected values of γ_1 were recorded. Accordingly, from the graph shown in Figure 11b, a plane corresponding to $QBAL = 11$ mL/min was selected. Points were searched in this plane so that the calculated value of γ_1 (from Eq. 30) were approximately the same as those γ_1 values recorded from graph 11a. These two sets of points were plotted in a $\gamma_2 \times \gamma_3$ plane shown in Figure 12. It can be seen that both strategies define the same separation area. Figure 13a shows the regions of separation found from both strategies in the same system of coordinates $(\gamma_1,\gamma_2,\gamma_3)$. Again, it is clear that both strategies convey the same information. Furthermore, *QBAL* is geometrically represented by planes standing in a 45° angle with respect to the $\gamma_2 = \gamma_3$ plane, as shown in Figure 13b.

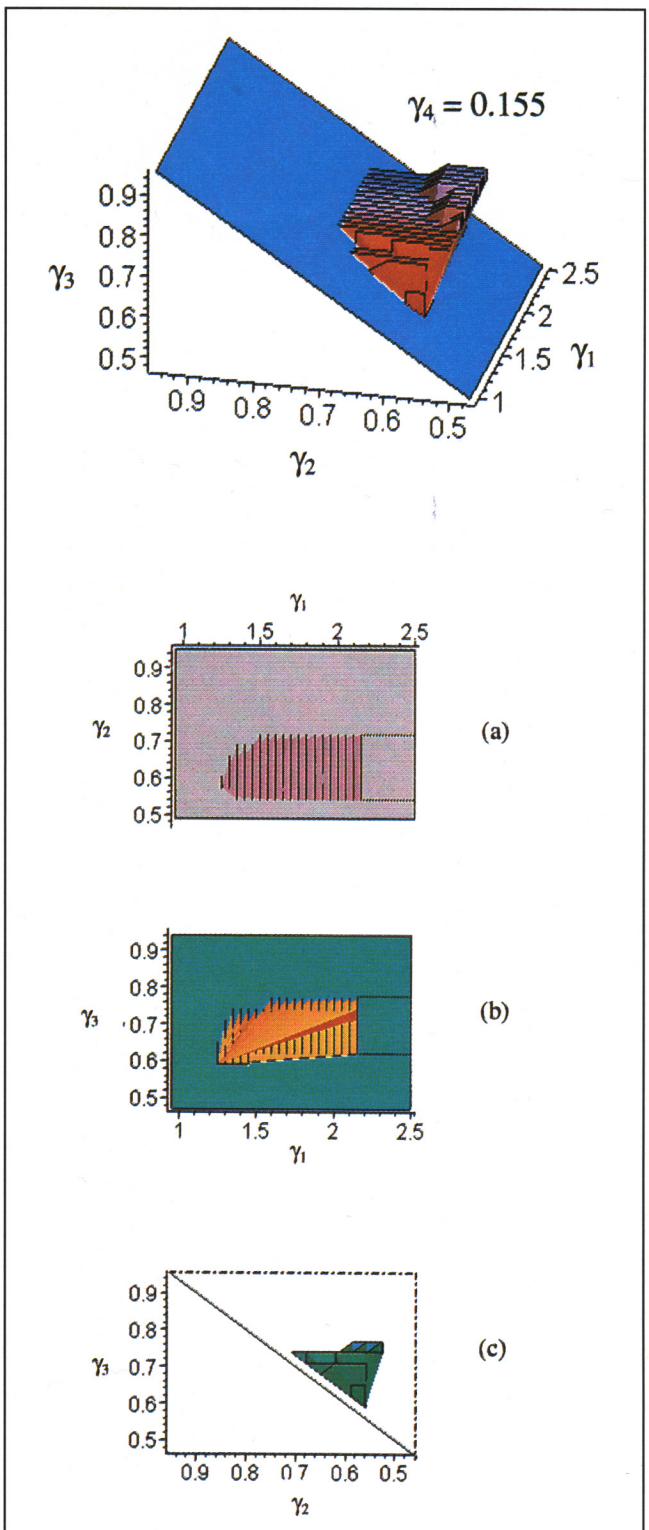

Figure 8. Separation volume in a $\gamma_1 \times \gamma_2 \times \gamma_3$ 3-D coordinate system for γ_4 = 0.155 and the corresponding 2-D projections on (a) γ_3, (b) γ_2, and (c) γ_1 planes, respectively.

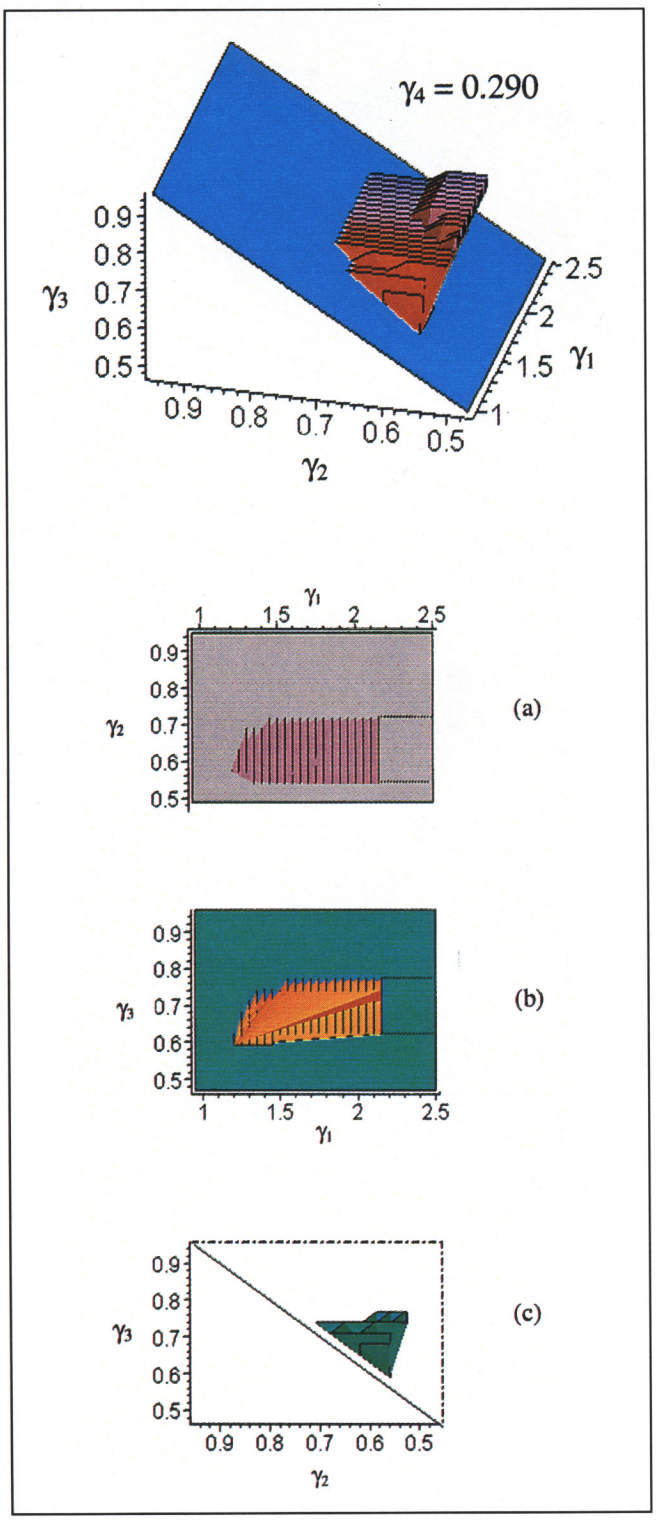

Figure 9. Separation volume in a $\gamma_1 \times \gamma_2 \times \gamma_3$ 3-D coordinate system for $\gamma_4 = 0.290$ and the corresponding 2-D projections on (a) γ_3, (b) γ_2, and (c) γ_1 planes, respectively.

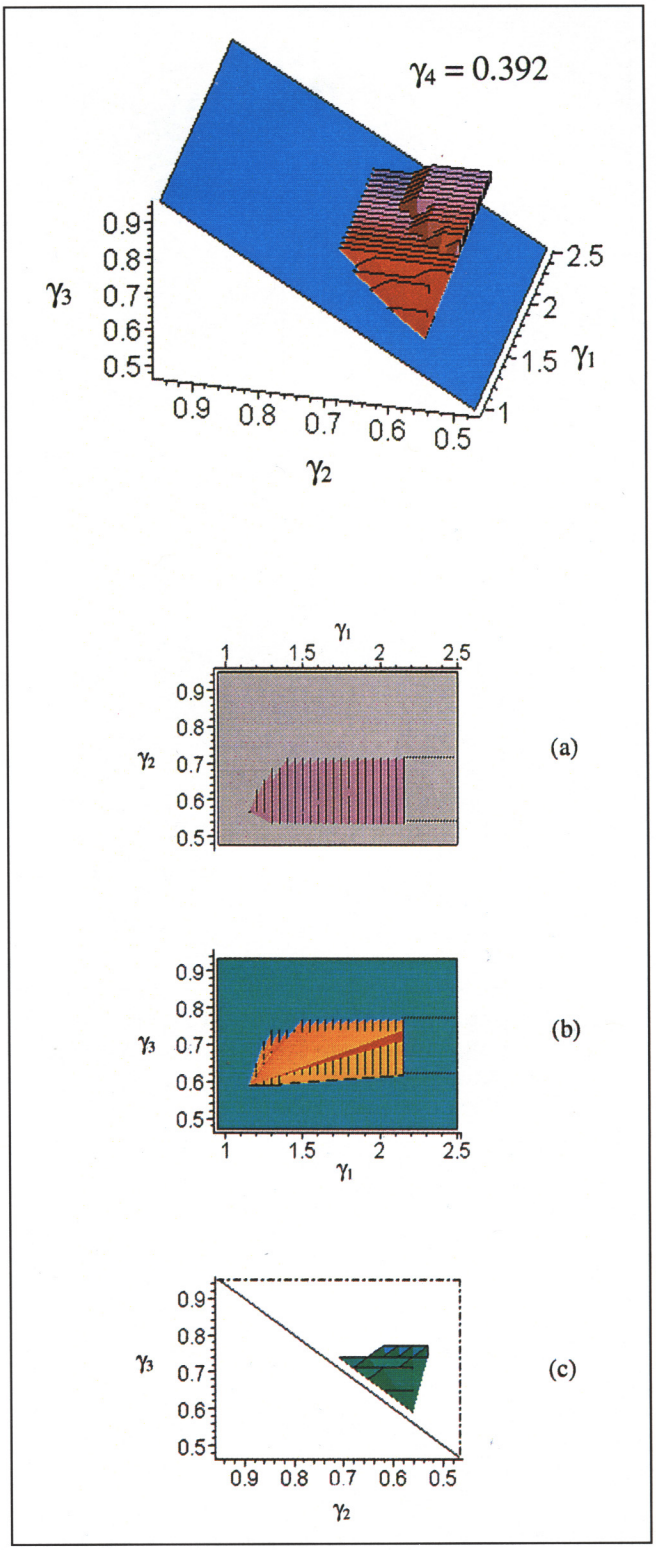

Figure 10. Separation volume in a $\gamma_1 \times \gamma_2 \times \gamma_3$ 3-D coordinate system for $\gamma_4 = 0.392$ and the corresponding 2-D projections on (a) γ_3, (b) γ_2, and (c) γ_1 planes, respectively.

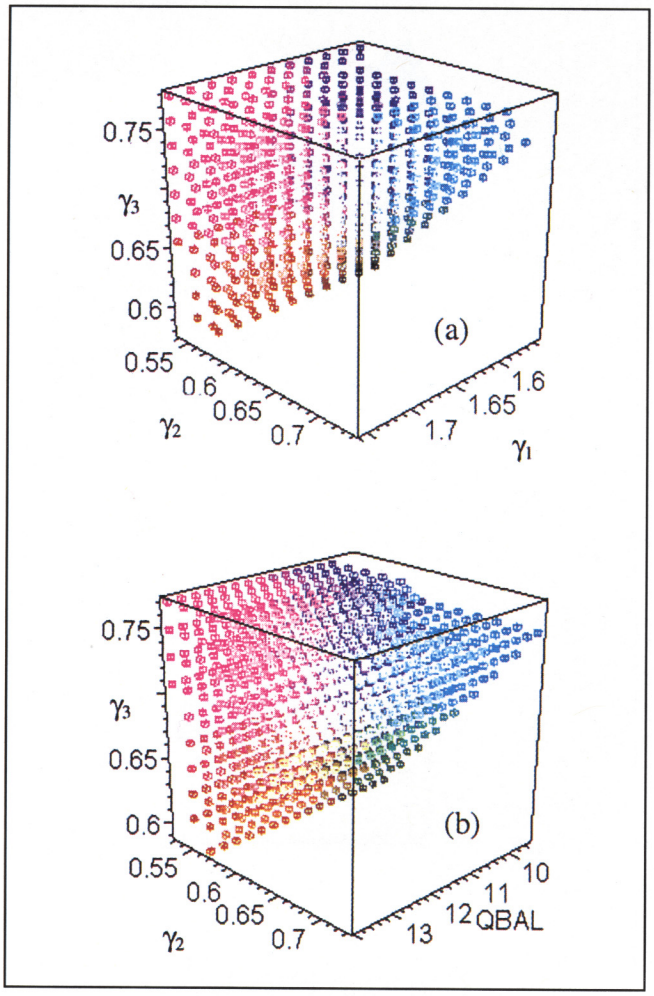

Figure 11. Regions of separation in a 3-D space found from (a) strategy 1 (γ_1 increments), and (b) strategy 2 (*QBAL* increments).

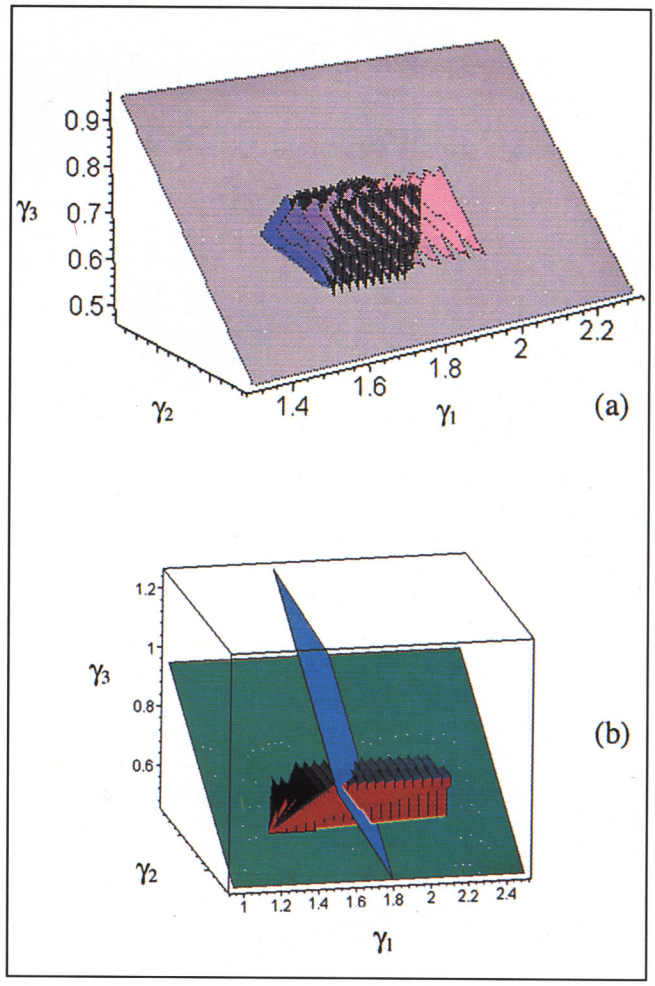

Figure 13. (a) Regions of separation from strategies 1 and 2; (b) blue plane standing at 45° with the $\gamma_2 = \gamma_3$ plane (green) is a region of constant *QBAL*, and the red surface is a region of separation as found from strategy 1 ($\gamma_4 = 0.290$; $\alpha_p = 200$; $\alpha_\mu = 12$).

The dark brown polygons, which are normal to the light gray plane ($\gamma_2 = \gamma_3$), were regions of separation found from strategy 1. The lilac/pink polygons, which form a 45° angle with the $\gamma_2 = \gamma_3$ plane, were found using strategy 2.

Conclusions

Optimizing the performance of a simulated moving-bed chromatographic separator is an essential step before operating an actual plant. When an ideal equilibrium model is used, the limiting flow-rate ratios required to achieve separation depend solely on equilibrium data. However, in the presence of mass-transfer effects, there is no explicit expression to define these limits. This work proposed two strategies of optimization for linear equilibrium binary mixtures that take mass-transfer effects into consideration. It was observed that the flow-rate ratio constraints on sections II and III of an SMB are dependent on the flow-rate ratios in neighboring sections, on the kinetic time constant, on zone length, and on the solid velocity. As a result, the limits of the region of separation in a $\gamma_2 \times \gamma_3$ plane may not be evaluated explicitly, but should be assessed through simulation. As expected, narrower ranges of $\gamma_2 \times \gamma_3$ values were found as compared to those predicted from an ideal equilibrium model. The influence of mass-transfer effects on the constraints of zones I

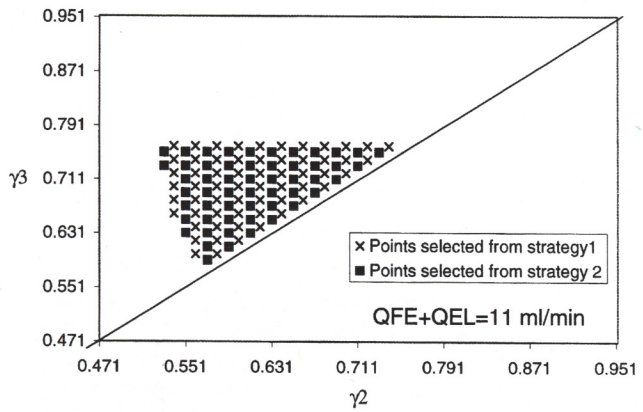

Figure 12. Comparison of points selected from both strategies of optimization for $QBAL = Q_F + Q_E = 11$ mL/min.

and IV was also evident from numerical simulations. Finally, the two proposed strategies to find the regions of separation in a three-dimensional space were proved to yield equivalent results.

Acknowledgments

Financial support from CAPES (proc. 1140/96), Ministry of Education of Brazil, and project PRAXIS XXI/33.1/CEG/2644/95 (Portugal) are gratefully acknowledged.

Notation

C = fluid-phase concentration, mole/bed volume
$\overline{C}_p$ = mean pore concentration, mole/vol. particle
D_c = column diameter, m
D_{pe} = effective pore diffusivity, m^2/s
K = equilibrium constant, pore vol./particle vol.
K' = equilibrium constant for a homogeneous adsorbent particle, pore vol./particle vol.
k = mass-transport coefficient (LDF), s^{-1}
k_f = film mass-transfer coefficient, m/s
k_p = mass-transport coefficient in the pores, s^{-1}
k_μ = mass-transport coefficient in the microparticles, s^{-1}
L_c = column length, m
$\langle \bar{q} \rangle$ = mean solid-phase concentration averaged over the particle, mol adsorbed/mass of particle
Q = fluid flow rate, m^3/s
$QBAL$ = sum of incoming or leaving flow rates ($Q_F + Q_E = Q_X + Q_R$), m^3/s
R_p = particle radius, m
t^* = rotation period, s
U_F = fluid interstitial velocity, m/s
U_S = solid interstitial velocity, m/s
V_c = column volume, m^3
ϵ = bed porosity, dimensionless
ϵ_p = particle porosity, dimensionless

Subscripts

c = column
F, R, E, X = feed, raffinate, eluent, and extract SMB streams, respectively
I, II, II, IV or $1, 2, 3, 4$ = subscripts referring to TMB zones
j = TMB/SMB section
p = particle
Rec = recycle

Literature Cited

Azevedo, D. C. S., and A. E. Rodrigues, "Bi-linear Driving Force Approach in the Simulation of Adsorptive Separation Processes: Application to Fixed and Simulated Moving Bed," *Proc. CHEMPOR'98*, Vol. II, F. Ribeiro and S. Alves, eds., p. 849 (1998).
Broughton, D. B., U.S. Patent No. 2,985,589 (1961).
Ernst, U. P. and J. T. Hsu, "Study of Simulated Moving Bed Separation Processes Using a Staged Model," *Ind. Eng. Chem. Res.*, **28**, 1211 (1989).
Fish, B. B., R. W. Carr, and R. Aris, "Optimization of the Countercurrent Moving-Bed Chromatographic Separator," *AIChE J.*, **39**, 1621 (1993).
Humprey, J. L., "Separation Processes: Playing a Critical Role," *Chem. Eng. Prog.*, **91**, 31 (1995).
Johnson, J. A., "Sorbex: Continuing Innovation in Liquid Phase Adsorption," *NATO ASI Adsorption: Science and Technology*, A. E. Rodrigues et al., eds., Kluwer, Amsterdam, p. 383 (1989).
Johnson, J. A., and R. G. Kabza, "Sorbex: Industrial-Scale Adsorptive Separation," *Preparative and Production Scale Chromatography*, G. Ganetsos and P. E. Barker, eds., Dekker, New York, p. 257 (1993).
Keller, G. E., II, "Adsorption: Building Upon a Solid Foundation," *Chem. Eng. Prog.*, **91**, 56 (1995).
Leão, C. P., L. S. Pais, M. Santos, and A. E. Rodrigues, "Simulated Moving Bed Adsorptive Reactor," *Process Intensification in Practice: Applications and Opportunities*, J. Semel, ed., BHR Group Conference Series 28, Antwerp, p. 143 (1997).
Ma, Z., and N.-H. L. Wang, "Standing Wave Analysis of SMB Chromatography: Linear Systems," *AIChE J.*, **43**, 2488 (1997).
Mazzotti, M., G. Storti, and M. Morbidelli, "Optimal Operation of Simulated Moving Bed Units for Non-Linear Chromatographic Separations," *J. Chromatog. A*, **769**, 3 (1997).
Mazzotti, M., G. Storti, and M. Morbidelli, "Robust Design of Countercurrent Adsorption Separation: 3. Nonstoichiometric Systems," *AIChE J.*, **42**, 2784 (1996).
Mian, L., D. C. S. Azevedo, and A. E. Rodrigues, "Protein Separation by SMB Chromatography: The Case of Non-Instantaneous Equilibrium at the Solid-Fluid Interface," PREP '99, San Francisco.
Pais, L. S., J. M. Loureiro, and A. E. Rodrigues, "Modeling Strategies for Enantiomer Separation by SMB Chromatography," *AIChE J.*, **44**, 561 (1998).
Pais, L. S., J. M. Loureiro, and A. E. Rodrigues, "Modeling, Simulation and Operation of a Simulated Moving Bed for Continuous Chromatographic Separation of 1,1′-bi-2-Naphthol Enantiomers," *J. Chromatogr. A*, **769**, 25 (1997).
Rosset, A. J., R. W. Neuzil, and D. B. Broughton, "Industrial Applications of Preparative Chromatography," *NATO ASI Percolation Processes: Theory and Applications*, A. E. Rodrigues and D. Tondeur, eds., Sithoff and Noordhoff, Alphen aan den Rijn, p. 249 (1981).
Ruthven, D. M., and C. B. Ching, "Counter-Current and Simulated Counter-Current Adsorption Separation Processes," *Chem. Eng. Sci.*, **44**, 1011 (1989).
Storti, G., M. Masi, S. Carrá, and M. Morbidelli, "Modeling and Design of Simulated Moving Bed Adsorption Separation Units," *Chem. Eng. Sci.*, **44**, 1329 (1989).
Storti, G., M. Mazzotti, M. Morbidelli and S. Carrá, "Robust Design of Binary Countercurrent Adsorption Processes," *AIChE J.*, **39**, 471 (1993).
Strube, J., U. Altenhöner, M. Meurer, H. Schmidt-Traub, and M. Schulte, "Dynamic Simulation of Simulated Moving Bed Chromatographic Processes for the Optimization of Chiral Separations," *J. Chromatogr. A*, **769**, 81 (1997).
Zhong, G., and G. Guiochon, "Analytical Solution for the Linear Ideal Model of Simulated Moving Bed Chromatography," *Chem. Eng. Sci.*, **51**, 4307 (1996).
Zhong, G., and G. Guiochon, "Steady-State Analysis of Simulated Moving-Bed Chromatography using the Linear, Ideal Model," *Chem. Eng. Sci.*, **53**, 1121 (1998).
Zhong, G., M. Smith, and G. Guiochon, "Effect of the Flow Rates in Linear, Ideal, Simulated Moving-Bed Chromatography," *AIChE J.*, **43**, 2960 (1997).

Appendix: Single-Section Countercurrent Moving-Bed Unit—Analytical Solution for a Dispersionless, Linear Equilibrium Binary System

Analytical solutions always provide good visualization of physical phenomena. For a TMB single section, as shown in Figure A1, where a binary linear equilibrium mixture is fed, the analytical solution may be readily available. If intraparticle mass transfer is described with a bi-LDF approximation, though, the analytical expression for the bulk fluid-phase concentration, $C(x)$, is so long and complex that important effects related to the mass-transfer resistances may not be clearly seen. Therefore, mass-transfer kinetics inside adsorbent particles will be described in terms of a single LDF approximation. For a moving bed with plug flow for both solid

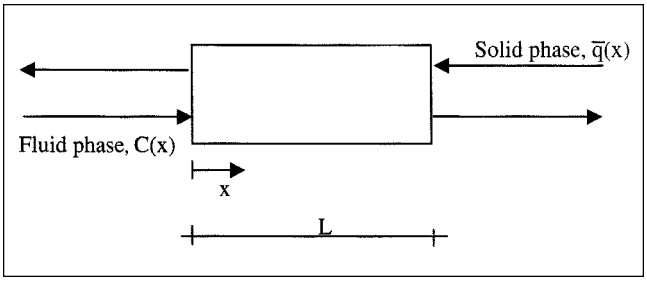

Figure A1. Countercurrent moving bed.

and fluid phases, the following equations are valid for the steady state:

$$\frac{dC}{dx} + \frac{\nu\alpha}{\gamma}(KC - \bar{q}) = 0$$

$$\frac{d\bar{q}}{dx} + \alpha(KC - \bar{q}) = 0$$

where

$$\alpha = \frac{k_p L}{U_S} \quad \text{and} \quad \bar{q} = \frac{\int_0^{R_p} q(R) R^2 \, dr}{\int_0^{R_p} R^2 \, dR}.$$

The analytical solution for the bulk fluid phase concentration is:

$$C(x) = C_1 + C_2 \exp\left(\frac{\alpha(\gamma - \nu K)}{\gamma} x\right),$$

where C_1 and C_2 are integration constants, which may be determined from the conditions at the boundaries. As in a four-section true moving bed, the boundary conditions in a given section are related to those in the previous and next section, and the solution for a single section was left undetermined.

Let us now examine what happens in sections II and III, where separation actually occurs. For separation to occur, A (in section III) and B (in section II) must move toward the feed port, as shown in Figure 4. For section II, the constraint on B (weakly adsorbed component) derived from the equilibrium theory is still true, so that

$$\gamma_2 > \nu K_B,$$

therefore

$$\frac{\alpha(\gamma_2 - \nu K_B)}{\gamma_2} > 0.$$

The concentration profile should be that of an exponential function of a positive number and the boundary conditions are those proposed by Ma and Wang (1997).

$$\begin{aligned} &\text{At } x = 0, && C_B(0) = C_B^{SS} \\ &\text{At } x = -\infty, && C_B(-\infty) = 0. \end{aligned}$$

For these boundary conditions, $C_1 = 0$ and $C_2 = C_B^{SS}$, so that

$$C_B^{II}(x) = C_B^{SS} \exp\left(\frac{\alpha(\gamma_2 - \nu K_B)}{\gamma_2} x\right).$$

If $C_B^{II}(x)$ is evaluated at the boundaries, that is, at $x = 0$ and $x = -1$, the following is true:

$$\beta_{B,II} = \frac{C_{B,II}(x = 0)}{C_{B,II}(x = -1)} = \exp\left(\frac{\alpha(\gamma_2 - \nu K_B)}{\gamma_2}\right),$$

and solving for γ_2,

$$\gamma_2|^{\min} = \frac{\alpha}{-\ln \beta_{B,II} + \alpha} \nu K_B = \frac{\alpha}{-\ln \beta_{B,II} + \alpha} \gamma_2|_{eq}^{\min}.$$

An analogous analysis will be done for species A in section III, since the equilibrium data for this component sets the upper limit of the region of separation in this section. In this case, the following boundary conditions apply:

$$\begin{aligned} &\text{At } x = 0, && C_A(0) = C_A^{SS} \\ &\text{At } x = \infty, && C_A(\infty) = 0. \end{aligned}$$

For these boundary conditions, $C_1 = 0$ and $C_2 = C_A^{SS}$, so that:

$$C_A^{III}(x) = C_A^{SS} \exp\left(\frac{\alpha(\gamma_3 - \nu K_A)}{\gamma_3} x\right).$$

The equilibrium constraint is also valid, so that

$$\gamma_3 < \nu K_A,$$

therefore

$$\frac{\alpha(\gamma_2 - \nu K_B)}{\gamma_2} < 0.$$

The profile of A in section III will be that of an exponential function of a negative number. If $C_A^{III}(x)$ is evaluated at the boundaries, that is, at $x = 0$ and $x = 1$, the following is true:

$$\beta_{A,III} = \frac{C_{A,III}(x = 0)}{C_{A,III}(x = 1)} = \exp\left(\frac{\alpha(\nu K_A - \gamma_3)}{\gamma_3}\right),$$

and solving for γ_3;

$$\gamma_3|^{\max} = \frac{\alpha}{\ln \beta_{A,III} + \alpha} \nu K_A = \frac{\alpha}{\ln \beta_{A,III} + \alpha} \gamma_3|_{eq}^{\max}.$$

Manuscript received Nov. 3, 1998, and revision received Feb. 11, 1999.